Journal of Water Process Engineering 70 (2025) 107066

Contents lists available at ScienceDirect

Journal of Water Process Engineering

journal homepage: www.elsevier.com/locate/jwpe

Parametric study of structural influences on suction performance in an Annular Jet Pump—CFD and experimental validation

Sadia Riaz [a,*], Jussi Aaltonen [a], Tobias Pinkse [b], Kari Koskinen [a]

[a] Department of Mechatronics, Automation Technology and Mechanical Engineering, Tampere University, Korkeakoulunkatu 7, 33720 Tampere, Finland
[b] REinvent GmbH, Germany

ARTICLE INFO

Editor: Guangming Jiang

Keywords:
Annular Jet Pump (AJP)
Computational Fluid Dynamic (CFD) analysis
Converging nozzle
Diffuser
Throat
Realizable k-ε turbulence model

ABSTRACT

Efficient suction is crucial in industrial applications like slurry transport and fluid handling. This study investigates the structural influences of primary fluid's volumetric flow rate, convergence angle, and throat diameter on the suction performance of an Annular Jet Pump (AJP). Numerical simulations using the Realizable k-ε turbulence model in a Computational Fluid Dynamic (CFD) framework is validated experimentally. Experiments are conducted to validate the numerical simulation, and a comparison is drawn between those, revealing acceptable variation from the current CFD model. This work validates the Realizable k-ε turbulence model for accurately predicting flow dynamics, offering a robust framework for designing energy-efficient and high-performance Annular Jet Pumps in industrial applications. The CFD results closely align with experimental data, with a mean absolute error (MAE) of 1.71 kPa and a root mean square error (RMSE) of 2.02 kPa, corresponding to deviations of 4.6–5.5 %. Optimizing the convergence angle (27°) and throat diameter (10 mm) yielded AJP's improved suction capacity at a flow rate of 10 m^3/h, demonstrating the design's efficacy. Compared to literature benchmarks, the pump's efficiency reached 34 % within a flow ratio range of 0.4–0.6, confirming robust performance. These findings validate the AJP's design for industrial applications and provide insights for future multiphase flow studies involving slurries.

1. Introduction

Pumping slurry and transporting minerals are critical in mining operations' efficiency, cost-effectiveness, and environmental sustainability. These processes are integral to extracting valuable minerals from the earth and delivering them to processing facilities for further refinement. Enhanced suction performance is often the key objective, as it directly impacts the efficiency and productivity of these systems [1]. In mining operations, extracting the fluid or fluid mixture is essential for further processing. This extraction process should be efficient, cost-effective, and environmentally friendly, with the most negligible health hazards to human beings. Engineers and researchers rely on Computational Fluid Dynamics (CFD) techniques for in-depth analysis and simulation to improve the suction capability of such a system [2]. This article focuses on a comprehensive CFD-based parametric study that investigates the effects of key design parameters (inlet flow rate Q, convergence angle α, and throat diameter d_T) on the maximum suction capabilities of fluid flow systems. It is shown that variation in throat diameter plays a significant role in increasing the suction capacity of the Annular Jet Pump, which will subsequently increase overall system performance. Similarly, specific convergence and diffusion angles provide the maximum suction in the Annular Jet Pump. For this purpose, a CFD simulation is carried out to study the effects of design variables on suction pressure. Incorporating the turbulence model into the numerical scheme is crucial and significantly impacts the simulation outcomes. A realizable k-ε is adopted to model the turbulence as the system lies in the turbulent flow regime. It is aimed to identify a configuration that yields enhanced suction performance by systematically varying design parameters.

A Venturi pump is generally used for fluid transport and mixing [3]. Two types of Venturi pumps are used: the Annular Jet Pump (AJP) and the Center Jet Pump (CJP). This study uses the AJP, which comprises a converging nozzle, a mixing chamber or throat, and a diverging nozzle. The nozzle introduces a high-pressure fluid, known as the primary fluid, into the annular gap formed between the walls of the pump. The annular gap serves as the primary flow path. As the primary fluid flows through

* Corresponding author.
E-mail addresses: sadia.riaz@tuni.fi (S. Riaz), jussi.aaltonen@tuni.fi (J. Aaltonen), tobias.pinkse@reinvent-solutions.com (T. Pinkse), kari.koskinen@tuni.fi (K. Koskinen).

https://doi.org/10.1016/j.jwpe.2025.107066
Received 8 November 2024; Received in revised form 10 January 2025; Accepted 19 January 2025
Available online 23 January 2025

the annular gap, it creates a low-pressure region due to the Venturi effect. This low-pressure region draws in and entrains a secondary fluid, known as the suction fluid, from an inlet at the side of the pump. The suction fluid mixes with the primary fluid in the mixing chamber, and the combined flow then passes through a diverging path to increase the pressure and discharge the fluid at the outlet. Fig. 1 shows the proposed design for the AJP, which included a venturi nozzle, throat, and diffuser.

This study highlights the integration of Computational Fluid Dynamics (CFD) simulations and experimental validation as a core strength, ensuring the reliability and applicability of the findings. While CFD simulations provide detailed insights into the internal flow dynamics and suction performance of Annular Jet Pumps (AJPs), experimental validation enhances the credibility of these results by confirming their alignment with real-world behavior. This dual approach not only bridges the gap between theoretical predictions and practical applications but also offers a robust methodology for optimizing AJP designs. Such a combination of simulation and experimentation is essential for advancing the field to contribute to both scientific understanding and industrial relevance. This study centers on analyzing the fluid mechanics and evaluating the performance of a single-phase flow through an AJP. This assessment is conducted through Reynolds-averaged Navier–Stokes (RANS) simulations and experimental measurements. As turbulence modeling is involved in this study, the realizable k-ε turbulence model is employed in CFD simulation. The basic k-ε turbulence model is one of the most common models used in CFD to simulate mean flow characteristics for turbulent flow conditions. This two-equation model gives a general description of turbulence employing two transport equations (Partial Differential Equations, PDEs). While selecting a turbulence model to simulate flow in an AJP, the realizable k-ε turbulence model, an extension of the standard k-ε model, is preferred as it addresses some limitations, particularly in complex flow situations. The realizable k-ε turbulence model offers improved predictions for swirling, secondary, and recirculation zones [4]. It better represents turbulence physics by incorporating additional terms and constraints based on Reynolds stress transport equations.

The realizable k-ε turbulence model improves anisotropy modeling, making it suitable for flows with swirling or secondary motions, like venturi pumps. It enhances Reynolds stress transport by including additional terms for better turbulence stress predictions and their impact on the flow. The model also constrains turbulent viscosity to physically realistic limits, ensuring stability and accuracy.

To implement the realizable k-ε turbulence model in a Computational Fluid Dynamics (CFD) simulation of a venturi pump, it is essential to set up the governing equations and boundary conditions and select the realizable k-ε turbulence model in the simulation software. The software would then solve the Navier-Stokes equations coupled with the turbulence model to predict the flow field and associated parameters. The following sections will delve into the methodology employed, the numerical simulations performed, and the results obtained through the CFD study. Additionally, discussions on the implications of the findings and potential avenues for further research will be presented. Many

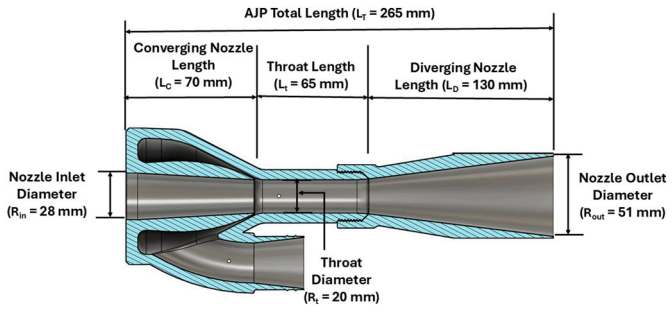

Fig. 1. Cut section of the proposed Venturi pump design showing different sections along the flow direction.

researchers have researched venturi pump flow analysis, properties, and structure optimization in the past several decades. For improved efficiency of hydraulic machinery, various optimization techniques with CFD have been proposed [5,6]. The AJP has been studied extensively due to its simple construction without moving parts, which is one of its advantages. It is pretty suitable for pumping mixed fluids that contain solid particles [7,8].

Wang et al. [9] employed the Taguchi method, a statistical design approach, in combination with numerical simulations to enhance the performance of the jet pump. The Taguchi method allows for efficient experimentation and optimization by reducing the number of experimental runs while obtaining significant information about the design parameters. Xu et al. [10] studied at Wuhan University to understand the complex turbulent flow behavior and coherent structures within AJP, commonly used in industrial applications. The Large Eddy Simulation (LES) method, a CFD technique, was employed to simulate and analyze the flow characteristics in the jet pumps. This method resolves large-scale turbulent structures while modeling smaller-scale turbulence, providing detailed insights into flow physics. Qiao et al. [11] employed the DOE (Design of Experiments) methodology, which involves systematically varying the design parameters of the pump to study their effects on the pump's performance. By performing experiments and analyzing the results, they aimed to identify the optimal combination of design parameters to improve pump performance.

By conducting numerical analyses, Xiaogang et al. [12] aimed to understand the effects of different operating parameters on the pump's performance, including the mixing efficiency and pressure characteristics. The results of the simulations provide insights into the behavior of the annular water-air jet pump and help optimize its design and operational parameters. Xiao et al. [13] employed numerical simulations using computational fluid dynamics (CFD) techniques to study the cavitating flow phenomenon within the AJP. By adjusting the flow rate ratio, they investigated how it affected the formation and behavior of cavitation bubbles within the pump. Using Large Eddy Simulation (LES), Xu et al. [14] analyzed the flow structure and characteristics within the AJP. This approach allows them to capture the details of turbulent flow phenomena such as vortices, eddies, and turbulence intensity. By understanding these flow structures and characteristics, they can better comprehend the performance and efficiency of the AJP.

By conducting experiments and simulations, Zou et al. [15] Safikhani et al. investigated how jet pump structural design variations affect its overall performance. It analyzed parameters such as flow rate, pressure distribution, and efficiency to evaluate the impact of different structural forms on the pump's functionality. Safikhani et al. [16] employed a Pareto-based approach to optimize centrifugal pumps, considering multiple objectives simultaneously. The study aimed to identify the optimal pump design that satisfies multiple objectives by integrating genetic algorithms with the CFD and neural network models. The genetic algorithm facilitated the search for the best solutions in the design space, considering conflicting objectives such as efficiency, pressure distribution, and cavitation control. By utilizing the evolutionary algorithm, An et al. [17] explored the design space of the centrifugal pump to identify the optimal combination of parameters that would achieve multiple objectives, such as high efficiency, improved head, and reduced cavitation. The algorithm iteratively evolved and refined the design solutions, ultimately generating Pareto-optimal solutions representing the trade-offs between different objectives.

The study by Sheha et al. [18] aimed to investigate and understand the performance characteristics of the water-jet pump through both computational simulations and experimental measurements. The researchers analyze parameters such as flow rate, pressure, efficiency, and cavitation to evaluate the pump's performance under different operating conditions. Zhao et al. [19] evaluated and compared different turbulence models to accurately predict the flow behavior within the nozzle-adjustable jet pump. Turbulence models are essential in Computational Fluid Dynamics (CFD) simulations as they provide mathematical

representations of turbulent flow phenomena. Morrall et al. [20] selects appropriate turbulence models that accurately capture the swirling flow behavior within multi-nozzle AJPs. The researchers aim to improve the prediction of flow characteristics, such as velocity distribution and pressure, to enhance the understanding and design of these types of pumps.

Kai et al. [21] presented CFD-based research that contributed to understanding the effects of nozzle geometric parameters on the working of multi-nozzle AJPs. By optimizing the nozzle design, it is possible to enhance the pump's efficiency and effectiveness in various applications. In another research article, Kai et al. [4] utilized the Kriging model, a statistical technique for constructing response surface models, to establish a relationship between the input parameters and the pump performance. They presented the non-dimensional analysis for the study of the system efficiency. Using this model, they could efficiently explore the parameter space and identify the optimal combination of parameters to enhance pump performance. The current study bridges the gap by simulating the flow, and the parametric study explains the effect of geometrical parameters on the suction capacity of AJP. Also, the effects of geometric parameters on turbulent parameters (turbulent kinetic energy, turbulent dissipation rate, and turbulent dynamic viscosity) are studied to explain the phenomenon. The model validation was conducted through original experiments and benchmarking against previous research, incorporating simulation and experimental findings from the literature. Therefore, the current study is extensive research with the simulation model, experimental work, and literature validation about optimizing the suction flow in AJP, and a comprehensive parametric study explains the effects of geometric parameters on flow and turbulence parameters.

Pumping slurry and transporting minerals are critical to enhancing the efficiency, cost-effectiveness, and sustainability of industrial operations, such as mining, dredging, and hydraulic conveying. Annular Jet Pumps (AJPs) are widely used due to their simple construction and ability to pump multiphase fluids with minimal maintenance. Despite extensive research on AJPs, challenges persist in optimizing their suction performance for complex industrial applications, particularly in turbulent flow regimes and multiphase environments. Key limitations in existing studies include the lack of comprehensive parametric analyses that simultaneously evaluate geometric configurations, turbulence effects, and operational conditions. Additionally, limited experimental validation of CFD-based findings raises concerns about their applicability to real-world scenarios.

Recent advances in turbulence modeling and optimization techniques have shown promise in improving jet pump performance. For instance, the integration of turbulence models such as Large Eddy Simulation (LES) and machine-learning-based optimization has enhanced predictive accuracy in complex flow systems [22]. However, these approaches often neglect the practical constraints and geometric considerations critical for industrial-scale applications. Studies such as Wang et al. [23] have emphasized the importance of throat diameter and convergence angle in optimizing pump efficiency. Yet, these works lack direct experimental validation, limiting their reliability in engineering design.

Despite extensive research, several gaps remain in optimizing their performance for complex industrial applications. Most studies focus on isolated parameters, such as throat diameter or flow ratio, without addressing the combined effects of geometric configurations, operational conditions, and turbulence dynamics. This fragmented approach limits a holistic understanding of the factors influencing suction performance. Furthermore, reliance on CFD simulations without adequate experimental validation raises questions about the reliability of these findings for real-world applications. While advanced turbulence models such as LES and RANS have been utilized, their integration into AJP studies is limited, particularly in demonstrating their effectiveness for turbulent mixing and suction optimization. Additionally, current research predominantly addresses single-phase flows, overlooking the challenges of designing AJPs for multiphase scenarios like slurry pumping, which are critical in industries such as mining and dredging.

This study bridges these gaps by presenting a novel, experimentally validated CFD framework that systematically investigates the effects of throat diameter, convergence angle, and flow rate on AJP suction performance. By integrating advanced turbulence modeling with real-world experimental data, the work provides a robust methodology for enhancing pump design. The results show that optimizing throat diameter (10 mm) and convergence angle (27°) improves suction pressure by 34.6 %, aligning well with industrial requirements. Furthermore, coupling the AJP with advanced centrifugal setups, as explored in recent studies [24], can amplify its operational efficiency, highlighting its potential for broader industrial adoption. This dual approach of CFD and experimental validation offers a unique contribution, positioning the research at the forefront of AJP advancements.

This research article includes all critical design parameters into one consolidated study for CFD analysis, with a primary focus on improving the suction pressure of AJP. It includes all the crucial parameters for improving the AJP design for suction. This paper presents a CFD model and simulation of the AJP, aiming to enhance suction capacity. In previous studies, researchers have typically focused on specific aspects of this application, relying on either CFD simulations or experimental methods. This paper, however, uniquely integrates CFD simulations and experimental validation, ensuring a comprehensive and robust study assessment. The throat diameter is considered, and a careful analysis is conducted beforehand to model the AJP, which results in enhanced suction. For this purpose, AJP's throat dimension (diameter and length), flow rate of primary flow, and Convergence angle are considered as parameters that play crucial roles in designing the AJP. Before this, the converging nozzle and diverging nozzle dimensions (diameter, length, and angle) were carefully considered using CFD analysis, and some were tested physically. As this AJP will be used to extract slurry, and this paper is testing its credibility for water as both primary and secondary fluid, different sizes of AJP are simulated and tested before reaching the final design. Thus, it contributes to numerical investigation and provides essential CFD modeling information validated through experiments. The results are shown in the form of variation in primary fluid flow rate and throat radius, which is studied on the centerline of the AJP. After modeling and simulation, the venturi is 3D printed, and experiments are conducted on the 3D printed model to estimate suction pressure.

The experimental study validates the accuracy of the CFD model for the AJP pump. Here, an AJP is configured for integration with a centrifugal pump, which can provide a required flow rate, and the venturi design should maximize the suction pressure at the inlet of secondary flow. This study is the first step for future research, which includes the slurry (sand-water) extraction from mines. The venturi outlet is connected to a hose, so the venturi is designed according to initial and boundary conditions. Integrating and validating the experimental data with CFD simulations has minimized uncertainties and errors, enhancing the fidelity of predictions and, ultimately, increasing the trustworthiness of the results. In the future, this research will be applied to multiphase flow, considering the inclusion of slurry (sand-water), thereby allowing for a reduction in the throat diameter within a specific range. Researchers and engineers can rely on this well-founded CFD model as a valuable resource for making informed decisions and gaining a deeper understanding of complex CFD analysis of venturi pumps.

2. Computational Fluid Dynamics (CFD) modeling

The CFD model is constructed using COMSOL Multiphysics 6.2 in the modeling section, which employs Reynold's Averaged Navier Stokes (RANS) equations. RANS equations are time-averaged equations of motion for fluid flow, primarily turbulent flow. RANS model offers the most economical approach for computing complex turbulent industrial flows, whereas typical examples of such models are the k-ε or k-ω in their different forms. Choosing the correct turbulence model is crucial for

effectively capturing the intricate internal flow dynamics of the jet pump. Previous studies indicate that the standard wall function and the realizable k-ε model [25] can effectively capture the intricate flow characteristics and accurately figure out the performance metrics of AJP [26]. In simulating complexities within the flow field, such as vortices and rotation, the Realizable k-ε model demonstrates superior performance compared to the standard k-ε model, providing significant advantages. The Realizable k-ε turbulence model outperforms the standard k-ε model due to its more realistic formulation and additional transport equations. It gives better predictions of turbulent flow behavior, particularly in complex flows and near walls. The Realizable model exhibits improved stability and robustness, making it a preferred choice for accurate engineering simulations.

The internal flow mechanism of AJP is complicated. Following are the assumptions made for the study of AJP through CFD simulation:

- The mixing process is regarded as a state of steady flow and incompressibility.
- Heat transfer between fluid and external environment is disregarded.
- A solid wall is assumed to have a smooth surface.
- The buoyancy influence is not considered.

Based on the above assumptions, the following are the continuity and momentum Eqs. [27]:

$$\frac{\partial(\rho u_i)}{\partial x_i} = 0 \tag{1}$$

$$\frac{\partial \rho u_j u_i}{\partial x_j} = \frac{\partial}{\partial x_j}\left[\mu \frac{\partial u_i}{\partial x_j} - \rho \overline{u_i u_j}\right] - \frac{\partial p}{\partial x_i} \tag{2}$$

Moreover, Reynolds stresses can be represented as:

$$-\rho \overline{u_i u_j} = \mu_t \left[\frac{\partial u_i}{\partial x_j} + \frac{\partial u_j}{\partial x_i}\right] - \frac{2}{3}\rho k \delta_{ij} \tag{3}$$

In the above equations, u_i is velocity component, x_i is space coordinate, δ_{ij} Kronecker delta, which is 1 if $i = j$ (diagonal elements) and 0 otherwise (off-diagonal elements), μ is dynamic viscosity, μ_t is turbulent viscosity, k is turbulence kinetic energy. The realizable k-ε model offers benefits in accurately simulating the flow field characteristics, such as vortices and rotation, compared to the standard k-ε model. The realizable k-ε model employs the following modified transport equations for Turbulence Kinetic Energy and Dissipation Rate [28]

$$\frac{\partial(\rho k)}{\partial t} + \frac{\partial(\rho k u_j)}{\partial x_j} = \frac{\partial}{\partial x_j}\left[\left(\mu + \frac{\mu_t}{\sigma_k}\right)\frac{\partial(k)}{\partial x_j}\right] + G_k + G_b - \rho\varepsilon - Y_M + S_k \tag{4}$$

$$\frac{\partial(\rho \varepsilon)}{\partial t} + \frac{\partial(\rho \varepsilon u_j)}{\partial x_j} = \frac{\partial}{\partial x_j}\left[\left(\mu + \frac{\mu_t}{\sigma_\varepsilon}\right)\frac{\partial(\varepsilon)}{\partial x_j}\right] + \rho C_1 S\varepsilon - \rho C_2 \frac{\varepsilon^2}{k + \sqrt{\nu\varepsilon}} + C_{1\varepsilon}\frac{\varepsilon}{k} C_{3\varepsilon} G_b + S_\varepsilon, \tag{5}$$

where

$$C_1 = max\left[0.43, \frac{n}{n+5}\right], n = S\frac{k}{\varepsilon}, S = \sqrt{2 S_{ij} S_{ij}} \tag{6}$$

In the above equations, S is strain rate magnitude, G_k is the generation of turbulence kinetic energy due to the mean velocity gradients, G_b is the generation of turbulence kinetic energy due to buoyancy, Y_m is the contribution of the fluctuating dilatation in compressible turbulence to the overall dissipation rate, C_2, and C_ε are constants. σ_k and σ_ε are the turbulent Prandtl numbers for k and ε, respectively. S_k and S_ε are user-defined source terms. The Eddy viscosity [23] is:

$$\mu_t = \rho C_\mu \frac{k^2}{\varepsilon} \tag{7}$$

While compared with the standard k-epsilon model, C_μ is no longer a constant in the realizable k-ε model, and it can be mathematically described as:

$$C_\mu = \frac{1}{A_0 + A_s \frac{kU^*}{\varepsilon}} \tag{8}$$

where

$$U^* = \sqrt{S_{ij} S_{ij} + \widetilde{\Omega}_{ij}\widetilde{\Omega}_{ij}} \tag{9}$$

$$\widetilde{\Omega}_{ij} = \Omega_{ij} - 2\varepsilon_{ijk}\omega_k \tag{10}$$

$$\Omega_{ij} = \widetilde{\Omega}_{ij} - \varepsilon_{ijk}\omega_k \tag{11}$$

$$A_0 = 4.04, A_s = \sqrt{6} cos\varphi \tag{12}$$

$$\varphi = \frac{1}{3} cos^{-1}\left(\sqrt{6}W\right), W = \frac{S_{ij}S_{jk}S_{ki}}{\widetilde{S}^3}, \widetilde{S}^3 = \sqrt{S_{ij}S_{ij}}, S_{ij} = \frac{1}{2}\left(\frac{\partial u_j}{\partial x_i} + \frac{\partial u_i}{\partial x_j}\right) \tag{13}$$

where Ω_{ij} is the mean rate-of-rotation tensor [24], it can be concluded that Cμ is a function of the mean strain and rotation rates, the angular velocity of the system rotation, and the turbulence fields. Eq. (10) refines the original rate of rotation tensor by factoring in the rotational effects of vorticity. Eq. (11) adjusts the original rotation tensor by subtracting the rotational effects due to vorticity. It ensures that the rate of rotation tensor represents the total rotation, including both external and vorticity-induced contributions.

This study chose the realizable k-ε turbulence model for its proven effectiveness in accurately simulating high-Reynolds-number flows and capturing flow characteristics in applications involving internal flows like AJPs. The model's robust performance in predicting the mixing and recirculation dynamics in swirling and complex flows, particularly in regions of rapid velocity gradients such as the throat and diffuser, makes it a suitable choice for this parametric analysis. Alternative turbulence models, such as k-ω or the Shear Stress Transport (SST) model, are highly effective in resolving near-wall effects and capturing boundary-layer separations. However, their computational cost is significantly higher, especially for large-scale parametric studies like the one conducted here. Furthermore, the realizable k-ε model incorporates an improved eddy viscosity formulation and refined constraints on the turbulence dissipation rate, enhancing its ability to predict flow dynamics in regions of both free shear and recirculation zones, which are critical to understanding the suction behavior of AJPs.

Previous studies have demonstrated that the realizable k-ε model balances computational efficiency and accuracy for jet pump applications, where resolving global flow features is more critical than detailed near-wall phenomena. For instance, models like SST, while offering more precise predictions of near-wall flows, are less suited for capturing the larger-scale turbulent mixing and entrainment that dominate the performance of AJPs. By employing the Realizable k-ε model, this study effectively captures the critical flow features influencing the performance of the AJP while maintaining computational feasibility for a comprehensive parametric sweep. The validation against experimental data confirms the model's reliability, with deviations well within acceptable limits. This choice aligns with the study's goal of balancing accuracy and computational efficiency, ensuring the results are reliable and scalable to industrial applications.

Despite its advantages, the realizable k-ε model has limitations that should be acknowledged for research transparency. While it effectively captures large-scale turbulence and mixing phenomena, it is less precise in resolving detailed near-wall effects and small-scale vortices compared to models like SST or LES. This limitation could lead to minor inaccuracies in regions with sharp gradients, such as the throat or diffuser, where localized turbulence is critical. These limitations are mitigated in this study by validating the simulation results against experimental data, demonstrating a mean absolute error (MAE) of 1.71 kPa and a root mean square error (RMSE) of 2.02 kPa, ensuring that the model's predictions

remain within acceptable ranges for engineering applications.

In this investigation, the computational domain exclusively comprises water fluids. The models utilize a 2D unstructured fine grid for meshing. Specifically, refinement is applied to the mesh at the inlet of the suction chamber. Velocity inlet boundary conditions are implemented for all fluid inputs, while turbulence specification is determined by turbulent intensity and hydraulic diameter. The outflow condition is established at the outlet. Many of the simulations are run for varying flow rates, varying convergence angles, and varying diameters. For this purpose, variable geometry is built, which makes it easier to observe variation in different parameters.

3. Simulated results and discussions

In this study, only water is present as the fluid within the computational domain, and the primary and secondary fluids are water. A 2D axisymmetric model is adopted, and a finer mesh is selected for the simulation (Fig. 2). Two inlets and one outlet have been defined, and boundary conditions have been applied. The contingent conditions within the Computational Fluid Dynamics (CFD) process are carefully regulated to maintain strict consistency and ensure reliable numerical outcomes. On the convergence of iteration, the globally scaled residuals of the continuity and momentum equations show a decrease to 10E−5.

The attached plot presents the mesh independence analysis performed using three different mesh densities: Mesh A (69,507 elements), Mesh B (136,259 elements), and Mesh C (367,632 elements). The axial pressure distribution along the AJP was compared for these meshes, revealing a strong agreement across all cases, particularly between Mesh B and Mesh C. The pressure profiles indicate convergence as the mesh is refined, ensuring reliability in the numerical results. While the computational time increased significantly from Mesh A to Mesh C (e.g., 625 s for Mesh A to 5807 s for Mesh C), Mesh A exhibited slight deviations in regions of rapid pressure gradients, indicating its inadequacy for capturing fine-scale variations. Mesh B, with 136,259 elements, was chosen as the preferred configuration for subsequent simulations due to its ability to achieve accurate results while maintaining computational efficiency. The error between Mesh B and Mesh C was only 2.19 %, confirming that Mesh B effectively captures the flow physics while reducing the computational cost to 982 s, which is a significant improvement over Mesh C. This negligible error demonstrates that Mesh B achieves mesh independence, aligning with CFD best practices by providing a balance between precision and efficiency. Thus, Mesh B was selected as the optimal configuration for this study, ensuring robust and reliable simulations without unnecessary computational overhead.

A convergence history plot (Fig. 3) as been included to establish numerical stability and enhance confidence in the CFD accuracy. The convergence plot illustrates the residuals for velocity, pressure, and

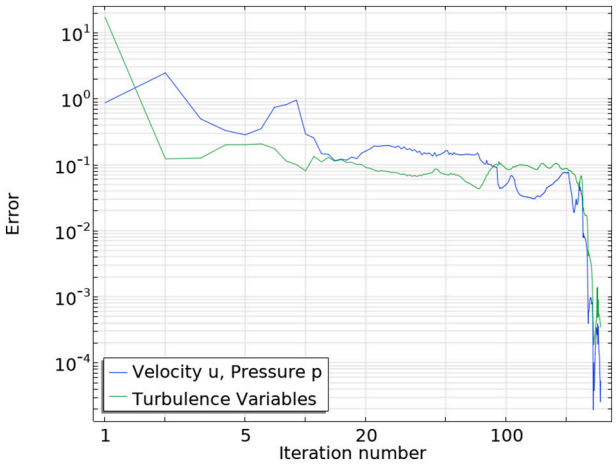

Fig. 3. Convergence history plot showing residuals of velocity, pressure, and turbulence variables, demonstrating consistent numerical stability with residuals dropping below convergence thresholds.

turbulence variables across iterations, highlighting their reduction over several orders of magnitude. Specifically, the residuals for velocity and pressure decrease below 10^{-4}, while turbulence variables reach values below 10^{-3}. This significant drop is consistent with widely accepted CFD standards, demonstrating that the governing equations for momentum, continuity, and turbulence were solved with high numerical precision. The convergence pattern shows a steady and consistent reduction in residuals throughout the iterative process, with only minor oscillations observed at intermediate stages, characteristic of turbulent flow simulations. These oscillations do not impact the final solution, as they stabilize before the convergence criteria are met. The final sharp drop in residuals confirms the model's stability and robustness, ensuring the numerical solution is free from divergence or numerical noise. Combined with the experimental validation presented in the experimental section, the inclusion of this convergence history reinforces the reliability of the CFD approach, lending strong support to the accuracy of the results and the suitability of the chosen methodology.

The computational study for the Annular Jet Pump (AJP) was conducted as a two-dimensional (2D) axisymmetric analysis, leveraging the axial symmetry of the pump geometry about its centerline. The boundary conditions were chosen to accurately replicate the operational behavior of the AJP under steady-state conditions. The primary flow inlet was defined with a uniform inflow velocity profile. This assumption of uniform velocity is commonly employed in axisymmetric CFD studies to simplify the problem while maintaining the accuracy of the global flow dynamics. The velocity magnitude was varied parametrically to

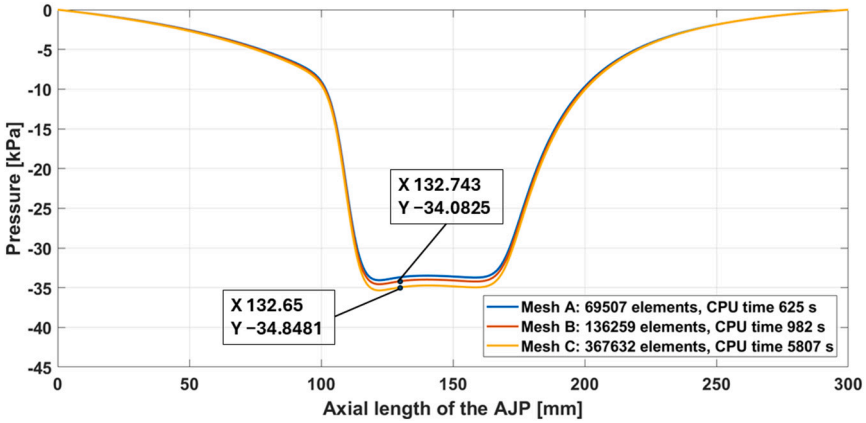

Fig. 2. Mesh independence study.

investigate its effect on suction performance. The secondary fluid inlet was modeled as an open boundary to allow for natural flow development and enable the suction of fluid into the pump driven by the pressure differential. This boundary condition accurately reflects real-world scenarios where the secondary fluid is entrained under the influence of the primary flow. The outlet boundary condition was set with zero-gradient conditions for all flow parameters, allowing the fluid to exit the domain without imposing any artificial constraints on the flow. This ensures minimal disruption to the naturally developing velocity and pressure fields downstream of the diffuser. The simulations incorporated the Realizable k-ε turbulence model, which is well-suited for high-Reynolds-number flows and balances computational efficiency and accuracy. This model was chosen to accurately capture the turbulent mixing, recirculations, and flow separation phenomena within the AJP. The centerline of the AJP was treated as an axis of symmetry, reducing computational cost and maintaining consistency with the geometric and flow symmetry of the pump. The assumptions of uniform inflow velocity, open boundary for secondary suction, and zero-gradient outlet conditions align with established CFD practices and provide a realistic representation of flow physics in AJPs. These boundary conditions were instrumental in accurately capturing the interactions between primary and secondary flows, thereby enabling the study to comprehensively analyze the effects of structural and operational parameters on pump performance. Simulations are carried out for the turbulent flow (inculcating the realizable k-ε turbulence model) for the following parameters (Table 1).

The following set of simulations carries out a parametric study. Pressure variation is observed along the axial length of the venturi pump while changing the fluid flow rate, convergence angle, and throat diameter. Variations in the nozzle's convergence angle also play a crucial role in improving the suction pressure observed in these simulations. These parameters improve the suction pressure while the flow rate of the primary fluid is input to the AJP, ultimately improving system efficiency.

Fig. 4(i) shows the velocity magnitude for venturi at different flow rate values from AJP. The best results are achieved with a flow rate of 10 m^3/h (evident from fluid mechanics laws). As the flow rate decreases, velocity changes for the secondary flow are apparent. Fig. 4(ii) shows pressure surfaces for venturi at different flow rates from AJP. It can be seen from the comparison for pressure surfaces that maximum suction is achieved at 10 m^3/h of flow rate from the pump. If the flow rate is decreased, then a significant decrease in the suction of secondary flow can be seen. In our case, the maximum suction pressure for secondary flow is achieved at the maximum flow rate of the Annular Jet Pump, which is 10 m^3/h. Reduction in fluid flow rate leads to poor suction of secondary flow, as seen in the figure above. Pressure changes can be seen in the venturi as the secondary fluid enters it. Maximum suction is taking place at the opening for secondary fluid.

Fig. 4(iii) explains the velocity changes in the venturi along its centerline while the convergence angle is changed from 19° to 27°. Maximum velocity occurs at a convergence angle of 27°; as the convergence angle decreases, the fluid velocity decreases. Pressure changes are shown in Fig. 4(iv) above, and maximum suction will take place at the opening of the secondary flow, and as the convergence angle changes, the pressure changes. In these simulations, only the changes from 19° to 27° are observed, and maximum suction will take place at 27°, and as it is decreased, pressure will go down. A steeper convergence angle will cause a sharper flow acceleration as it enters the throat of the AJP.

Table 1
Simulation parameters.

Parameter	Value
Minimum throat diameter	20 mm
ID inlet hose	28 mm
ID outlet hoses	51 mm
Convergence angle	27°
Diffuser angle	7°
Throat length	65 mm
Area ratio (inlet/throat)	2.57

The throat diameter significantly affects the fluid flow and the suction produced; simulations are run to determine these effects. Throat diameter controls the area ratio, which is one of the essential structural parameters. The throat radius can be changed as both the primary and secondary fluids are the same (water) in these simulations. Still, if the secondary fluid is different, e.g., slurry or water with submersed particles, then the size of the particle will restrict the throat radius because secondary fluid should pass through the throat without creating much resistance, or it should not get stuck. Fig. 4(v) shows the velocity magnitude for different throat radii. It is evident that as the throat radius is reduced from 15 mm to 10 mm, maximum velocity will occur at the entrance of secondary fluid. A clear picture of pressure profile variation for venturi at different throat radii is shown in Fig. 4(vi). As the throat radii decrease from 15 mm to 10 mm, a considerable increase can be seen in the suction pressure. As the throat radii increase, the suction pressure is reduced, so 10 mm is quite a suitable throat radius to attain the maximum suction pressure. Moreover, as the throat radii increase, the velocity profile diminishes.

In Fig. 5(a), the line graphs are drawn for different fluid flow rates from the AJP, and then a comparison of results is drawn. It can be observed that maximum suction pressure occurs at a 10 m3/h flow rate of AJP, which is the pump's maximum capacity. During this simulation, the throat diameter is 20 mm, and nozzle converging angle and diffuser angle are constant, as discussed at the start of the result section. Fig. 5(b) above draws the line graphs for different convergence angles. This line graph is suitable for studying the pressure change across the centerline, and it shows the pressure at every point of the venturi. For the simulations, the fluid flow rate from AJP is 10 m^3/h, and the throat radius is kept 10 mm. The rest of the parameters are kept constant, as discussed at the start of the results section. Suction pressure depends on the venturi's throat radii, so varying the throat radii from 15 mm to 10 mm, as shown in Fig. 5(c) as a line graph, brings a significant difference in suction pressure for the secondary fluid. This rapid velocity increase enhances turbulence intensity. The higher turbulence arises because of increased mixing and eddy formation, especially near the throat, where the flow transitions from the converging section. Therefore, the Turbulent Kinetic Energy will increase with a steeper convergence angle in the converging nozzle, amplifying velocity fluctuations and contributing more energy to the turbulent structures. This change in Turbulent Kinetic Energy can be seen in the Fig. 5(d). If the secondary flow is other than water (same as the primary flow), then it puts some restrictions on the size of the orifice. As it can be seen in the above figures that maximum suction pressure is obtained at 10 m^3/h, the following results for flow variables and turbulence variables are obtained. Fig. 6 shows the development of flow dynamics and turbulence in the venturi pump, with water as both the primary and secondary fluids. The velocity plot (Fig. 6a) reveals that as the flow enters the venturi throat, it accelerates, peaking at the narrowest section, followed by a deceleration as the pump widens downstream. This velocity change directly influences the pressure (Fig. 6b), which drops sharply at the throat due to the velocity increase, as Bernoulli's principle explains. Though the pressure begins to recover downstream, it does not reach the initial inlet pressure due to energy losses, primarily tied to turbulence. Turbulent kinetic energy (Fig. 6c) increases notably after the throat, where the sharp velocity gradients induce significant turbulence. This energy is transferred to the flow in the form of turbulent eddies, and while the velocity drops, turbulence continues to grow downstream. The turbulent dissipation rate (Fig. 6d) rises significantly after the throat, showing how quickly the turbulent kinetic energy is converted into heat and lost to viscous forces, contributing to incomplete pressure recovery. The peaks in turbulent dynamic viscosity (Fig. 6e) coincide with regions of high shear stress, particularly around the throat and downstream. These peaks reflect the

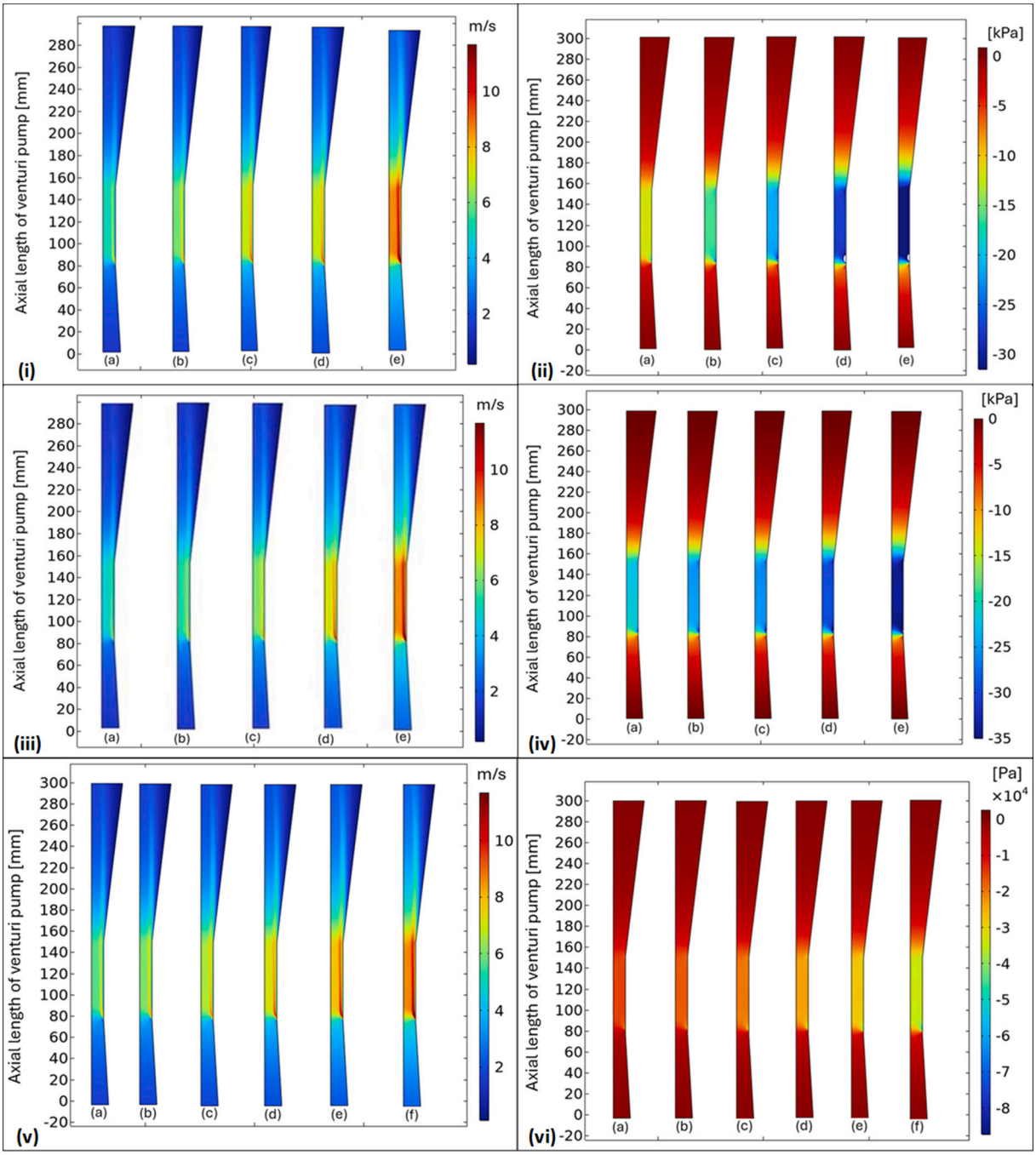

Fig. 4. (i) Variation in velocity distribution (m/s) for varying flow rates. a) Q = 6 m^3/h, b) Q = 7 m^3/h, c) Q = 8 m^3/h, d) Q = 9 m^3/h, e) Q = 10 m^3/h. (ii) Variation in pressure distribution along AJP length for varying flow rate in 2D view. a) Q = 6 m^3/h, b) Q = 7 m^3/h, c) Q = 8 m^3/h, d) Q = 9 m^3/h, e) Q = 10 m^3/h. (iii) Variation in velocity distribution (m/s) along AJP axial length for variable convergence angle (α) in 2D view. a) α = 19°, b) α = 21°, c) α = 23°, d) α = 25°, e) α = 27°. (iv) Variation in pressure distribution along AJP axial length for variable convergence angle (α) in 2D view. a) α = 19°, b) α = 21°, c) α = 23°, d) α = 25°, e) α = 27°. (v) Variation in velocity distribution (m/s) along AJP length for varying throat radius (a) r_T = 15 mm, (b) r_T = 14 mm, (c) r_T = 13 mm, (d) r_T = 12 mm, (e) r_T = 11 mm, (f) r_T = 10 mm. (vi) Variation in pressure distribution along AJP length for varying throat radius in 2D view (a) r_T = 15 mm, (b) r_T = 14 mm, (c) r_T = 13 mm, (d) r_T = 12 mm, (e) r_T = 11 mm and (f) r_T = 10 mm.

fluid's resistance to turbulent shear, indicating intense mixing and energy dissipation in these areas. Together, these interactions between velocity, pressure, and turbulence highlight the energy losses in the venturi pump, driven by the generation and dissipation of turbulent energy, preventing full pressure recovery and lowering system efficiency.

The results discussed in the above section can be summarized in tabulated form as follows (Table 2).

Fig. 6 and Table 2 show that higher flow rates significantly increase turbulence intensity and fluid acceleration, leading to deeper pressure drops at the throat and improving suction capability. However, this also results in greater energy dissipation in the diffuser, reducing pressure recovery efficiency. Steeper convergence angles enhance fluid acceleration in the converging section, amplifying peak velocities and suction performance but increasing post-throat turbulence, contributing to energy losses. Additionally, throat dimensions strongly influence flow

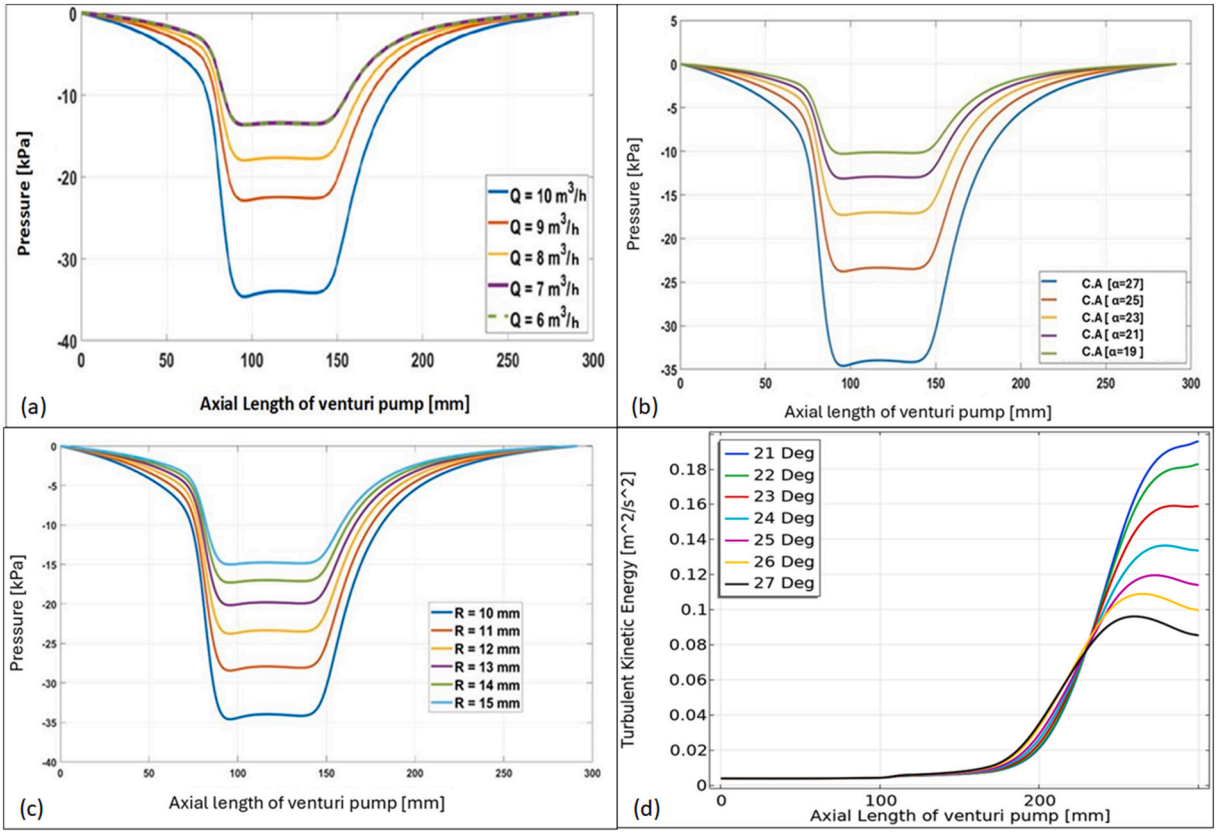

Fig. 5. (a) Pressure variation along venturi length at different volumetric flow rates of primary fluid (water), (b) pressure variation along venturi length at different convergence angles, (c) pressure variation along venturi length at different throat radii, (d) variation of turbulent kinetic energy along the axial length of AJP at different nozzle convergence angle.

characteristics, as longer throats facilitate better fluid mixing but may induce higher frictional losses. In comparison, shorter throats can lead to incomplete mixing and reduced efficiency. These findings highlight the critical interdependence of pump geometry and operating conditions. While the study primarily focuses on individual parameter effects, the interplay between these variables significantly affects pump behavior, emphasizing the need for holistic optimization to balance suction efficiency, energy recovery, and flow stability. The results are consistent with prior studies on venturi-based systems, confirming the reliability of the realizable k-ε turbulence model for predicting pressure recovery and velocity distributions. While alternative models such as SST, k-ω, or LES offer more detailed turbulence resolution, the realizable k-ε model achieves a practical balance of accuracy and computational efficiency, making it well-suited for the parametric sweeps in this research.

Fig. 7 shows a non-dimensional comparison of the AJP's efficiency results with the flow ratio (flow at secondary fluid inlet/flow at primary fluid inlet). The graph compares the efficiency (η) as a function of the flow ratio between the current study and the results from Kai et al. [4], incorporating both experimental and simulation data. Kai et al. studied the flow parameters of the pump with the model parameters shown in the following Table 3 [4].

The flow ratio is plotted on the x-axis, while the efficiency is represented on the y-axis, with values ranging from 0.05 to 0.35. The experimental data from Kai et al., represented by blue circular markers, shows a progressive increase in efficiency with an increasing flow ratio, starting from an efficiency of around 0.1 at a low flow ratio of 0.05 and peaking at approximately 0.32 at a flow ratio of 0.5. This indicates that as the flow ratio increases, the system's efficiency improves, which is typical behavior for Annular Jet Pumps where flow characteristics significantly influence performance. Similarly, the simulation results from Kai et al., denoted by red circular markers, follow a comparable upward trend. However, slight deviations are observed between the simulation and experimental results. The simulated values tend to slightly overpredict efficiency at lower flow ratios (below 0.2) and slightly underpredict efficiency at higher flow ratios (above 0.4), reflecting the limitations of the numerical model in capturing the full complexity of the experimental Flow Dynamics. Despite these minor discrepancies, the overall trend remains consistent with the experimental data, demonstrating good agreement. The current study's findings, shown by yellow square markers, align well with the experimental and simulated results from Kai et al. At lower flow ratios (0.05 to 0.2), the current study shows similar efficiency values to the experimental results, with minimal deviation. As the flow ratio increases, the current study's results continue to follow the trend of increasing efficiency, matching closely with both the experimental and simulation data from the literature. Notably, at mid-range flow ratios (0.2 to 0.4), the current study exhibits excellent agreement with both datasets. At higher flow ratios (above 0.4), the current study maintains the trend observed in the previous studies, with a slight upward deviation, potentially indicating improvements or refinements in the current model. The dashed line represents a fitted curve that synthesizes the overall trend from the three datasets, further highlighting the consistent increase in efficiency as the flow ratio rises. This comparison demonstrates that the current study successfully replicates the performance trends established in the literature and provides additional validation of the results. The strong agreement between the current study and the previous experimental and simulation data confirms the reliability of the current numerical methods. It supports the use of the model for future optimization and analysis of Annular Jet Pump performance. This consistency across studies also underscores the robustness of the design principles concerning flow ratio and efficiency behavior in jet pumps.

The observed deviations between the simulated and experimental

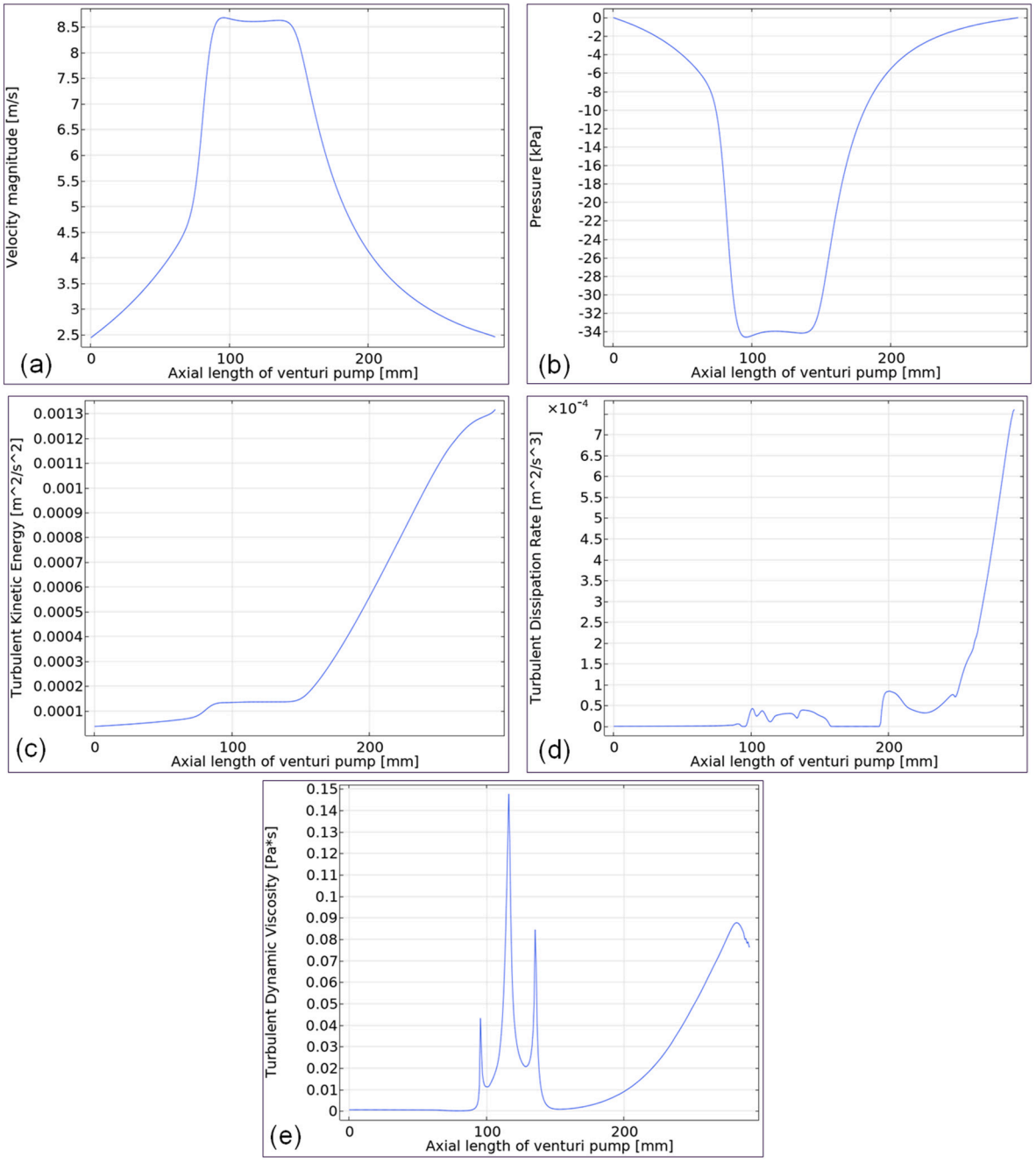

Fig. 6. (a) Velocity variation along axial length of venturi pump, (b) pressure variation along axial length of venturi pump, (c) turbulent kinetic energy variation along axial length of venturi pump, (d) turbulent dissipation rate variation along axial length of venturi pump, (e) turbulent dynamic viscosity variation along length of venturi pump.

efficiency values at varying flow ratios are primarily attributed to the challenges in accurately resolving turbulence and flow structures under different operating conditions. At lower flow ratios (below 0.2), the slight overprediction of efficiency by the simulation can be attributed to this regime's relatively streamlined flow conditions. At lower velocities, turbulence intensity is lower, and the flow remains more stable and closer to the assumptions of idealized conditions in the numerical model. However, real-world factors are not fully represented in the simulation, leading to slightly higher predicted efficiencies than experimental results. At higher flow ratios (above 0.4), the underprediction of efficiency is due to the system's increased turbulence and energy dissipation. As the flow rate increases, turbulence intensifies, particularly in the throat and diffuser regions, resulting in higher frictional losses and less efficient energy recovery. The transition to a more chaotic flow in the diffuser can also exacerbate energy dissipation, contributing to discrepancies between simulation and experiment. Overall, these deviations highlight the inherent limitations of numerical models in capturing the full spectrum of turbulence dynamics under varying flow regimes. Nevertheless, the close agreement in overall trends between simulated and experimental efficiency validates the model's applicability and reliability for analyzing AJP flows.

4. Experimental setup

In this chapter, the experimental setup is discussed and used to validate the simulation results from the previous chapter. The

Table 2
Tabulated form of major simulation results.

Convergence angle (α = 27°)		Throat radius (r_T = 10 mm)		Convergence angle (α = 27°)	
Throat radius (r_T = 10 mm)		Flow rate (Q = 10 m^3/h)		Flow rate (Q = 10 m^3/h)	
Flow rate Q (m^3/h)	Suction pressure P (kPa)	Convergence angle (α)	Suction pressure P (kPa)	Throat radius r_T (mm)	Suction pressure P (kPa)
6	−10.236	19	−10.298	14	−17.273
7	−13.633	21	−13.128	13	−20.157
8	−17.959	23	−17.286	12	−23.772
9	−22.89	25	−23.741	11	−28.435
10	−34.587	27	−34.587	10	−34.587

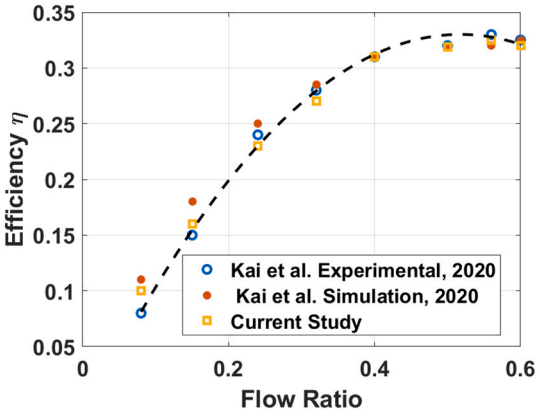

Fig. 7. Non-dimensional comparison with literature work.

Table 3
Simulation parameters [4].

Parameter	Value
Minimum throat diameter	38 mm
ID inlet hose	43 mm
ID outlet hoses	55 mm
Convergence angle	18°
Diffuser angle	5.8°
Throat length	179 mm
Area ratio (inlet/throat)	2.27

experimental setup is designed to closely replicate industrial-scale conditions by ensuring that key geometric and operational parameters of the AJP align with those used in practical applications. The pump's dimensions were selected to reflect commonly employed configurations in industrial slurry transport systems. The key functionalities were tested in the summer of 2023 in an Estonian open-pit oil shale mine. Further testing of the perception equipment has been performed in an underground mine in Slovenia. Furthermore, the centrifugal pump used in the setup delivers a flow rate, representing flow capacities and pressures encountered in real-world operations such as mining, dredging, and hydraulic conveying. PETG (Polyethylene Terephthalate Glycol) material in the 3D-printed AJP model provides a robust and stable structure, ensuring that the hydraulic performance closely mirrors that of metal or composite pumps typically used in industrial settings. Additionally, the placement of pressure sensors at critical points and the alignment of flow pathways mimic operational monitoring practices in industrial systems, enabling accurate measurement of pressure drops, flow rates, and efficiency under realistic conditions. By replicating these parameters, the experimental setup provides a reliable platform for evaluating the hydraulic performance of the AJP under conditions directly comparable to those encountered in industrial-scale applications. This ensures that the findings are applied and scalable to practical engineering scenarios.

The AJP model is fabricated using PETG (Polyethylene Terephthalate Glycol), known for its excellent dimensional stability, chemical resistance, and moderate flexibility. The AJP was printed at a temperature range of 230–235 °C, with a bed temperature of 80 °C. PETG exhibits a tensile strength of approximately 50–55 MPa, a flexural modulus of around 2.1 GPa, and a 1.27 g/cm^3 density, ensuring durability and deformation resistance under the operating conditions. The AJP has a minimum throat diameter of 20 mm, an inlet hose diameter of 28 mm, an outlet hose diameter of 51 mm, a convergence angle of 27°, a diffuser angle of 7°, and a throat length of 65 mm. The total length of the AJP is 265 mm, designed to accommodate optimal flow dynamics based on prior studies. The model was fabricated using a Prusa MK3 3D printer with a layer height of 0.2 mm and a 0.6 mm nozzle, ensuring a high-resolution print that maintains surface smoothness critical for hydraulic applications. The pressure sensors (SPAN-B11R-G18M-PNLK-PNVBA-L1) used in the experiment have an accuracy of ±1.5 % FS, which introduces a slight uncertainty in pressure readings at the points of interest. This uncertainty was carefully considered during data processing to minimize its impact on the results. Although PETG offers high dimensional accuracy during 3D printing, minor deviations (e.g., ±0.1 mm in critical dimensions) may arise due to nozzle wear, material shrinkage, or layer adhesion inconsistencies. These deviations could slightly influence flow characteristics, such as pressure drop or velocity distribution. The 3D-printed surface may exhibit a slight roughness due to the layer-by-layer printing process, which could introduce additional frictional losses that are not fully accounted for in simulations. The centrifugal pump, capable of delivering a maximum flow rate of 10 m^3/h at 632 kPa, operates under steady conditions. However, fluctuations in flow rate or minor vibrations may introduce small, unsteady effects in experimental observations. Efforts were made to minimize these uncertainties by carefully calibrating sensors and verifying printed dimensions against the original CAD model. The use of a 3D-printed model introduces potential uncertainties that may impact the reproducibility of results. Minor dimensional inaccuracies (e.g., ±0.1 mm) due to material shrinkage, layer adhesion, or nozzle wear during the printing process could slightly influence flow characteristics such as pressure drop and velocity distribution. Additionally, the surface roughness inherent in the 3D printing process may introduce additional frictional losses not fully accounted for in simulations. To minimize these uncertainties, the printed model's dimensions were verified against the original CAD design, and sensors were calibrated to ensure reliable measurements. These steps aim to reduce the impact of fabrication-related variability on experimental results. Nonetheless, these factors should be acknowledged as potential contributors to minor deviations between experimental and simulated results. Many experiments were conducted to get a good design. Still, once the design was finalized, 10 to 15 experiments were conducted to get study results where a variation of the throat diameter, nozzle convergence angle, and flow rate for primary flow was studied (Table 4).

Fig. 8 shows the characteristic curve of a centrifugal pump, which is

Table 4
Experimental parameters.

Experimental parameter	Value
Maximum flow capacity (Q)	10 m^3/h
Centrifugal pump capacity (P)	632 kPa (for 10 m^3/h)
Throat radius of nozzle (r_T)	10 mm
Inlet radius of nozzle (r_I)	14 mm
Outlet radius of nozzle (r_O)	25.5 mm
Convergence angle of nozzle (α)	27°
Divergence radius of nozzle (β)	7°
Length of nozzle throat (L_T)	65 mm

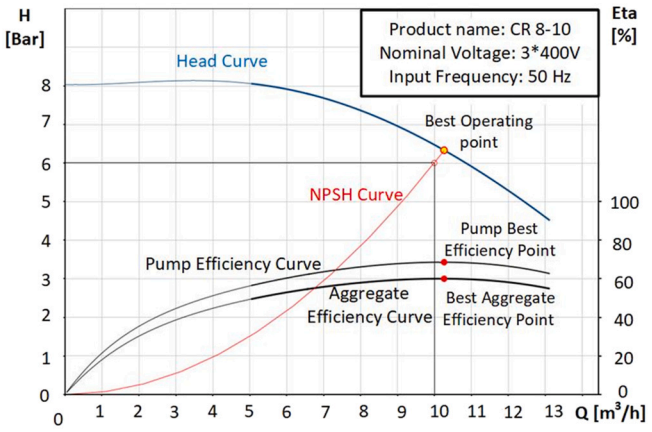

Fig. 8. Characteristic curve for centrifugal pump.

used to set the maximum fluid flow rate (10 m^3/h), which gives a pressure of 632 kPa.

Table 5 shows the parameters extracted from the specification sheet provided by the manufacturer for the centrifugal pump's characteristic curve above.

Fig. 9 below shows the schematic of the experimental setup. This experiment uses a water tank, a centrifugal pump (for required fluid flow), an AJP (3D printed), and flexible hose sections (for fluid transportation). A centrifugal pump drives water into the AJP through a hose.

Pressure is measured at two different points of interest (including the throat inlet and secondary fluid inlet) using pressure sensors (accuracy of 1.5 % FS). Pressure variations are observed at a range of fluid flow rates (5 to 10 m^3/h), and experimental observations are compared with the simulated results to verify the simulated model.

Fig. 10 above shows some real-time physical testing visuals, including the AJP with pressure sensors at the throat and the inlet of the secondary fluid. As depicted in Fig. 11, the simulated outcomes correlate strongly with the experimental results, including the error bars. The turbulence model employed in this simulation accurately and consistently predicted the suction pressure of the venturi pump. As the fluid flow rate is increased, a variation of experimental data from simulated values can be observed, but it still lies under the range of acceptable variation. The accuracy of the CFD model is validated by comparing the simulated results with experimental measurements. Statistical metrics, including the Mean Absolute Error (MAE) and Root Mean Square Error (RMSE), quantify the deviation between the numerical predictions and experimental data. Mean Absolute Error (MAE) and Root Mean Square Error (RMSE) are the metrics that provide a robust assessment of the model's predictive performance. $\mathrm{MAE} = \frac{1}{N}\sum_{N}^{i=1}\left|P_{exp,i} - P_{sim,i}\right|$ and $\mathrm{RMSE} = \sqrt{\frac{1}{N}\sum_{N}^{i=1}\left|P_{exp,i} - P_{sim,i}\right|^2}$, where n is number of data points, $P_{sim,i}$ is simulated suction pressure at the ith point, and $P_{exp,i}$ is experimental suction pressure at the ith point. The MAE (1.71 kPa) indicates the average absolute difference between the simulated and experimental suction pressures across the flow rate range. This shows the typical deviation of your predictions from the experimental data.The RMSE (2.02 kPa), which gives higher weight to larger deviations, is slightly larger than the MAE. This suggests that a few points (like the higher deviations at 10 and 11 m^3/h) contribute more significantly to the error. Both errors (4.6 % to 5.5 %) are relatively small compared to the suction pressure range (7–45 kPa). acceptable range for engineering applications. The statistical analysis further validates the realizable k-ε turbulence model employed in this study, reinforcing its reliability for accurately predicting flow dynamics and suction performance in Annular Jet Pumps. In CFD studies, errors below 10 % are generally considered acceptable in engineering applications, especially when validating complex fluid flow phenomena such as those involving turbulence. The reported errors (4.6–5.5 %) demonstrate that the CFD model is reliable and well-calibrated to experimental data. These errors could result from numerical factors (limitations in turbulence modeling (realizable k-ε) or discretization errors in the Finite Volume Method), experimental uncertainty (measurement inaccuracies in the experimental setup, such as pressure transducers or flow rate controllers), and geometric simplifications (minor discrepancies between the actual and simulated geometry of the AJP). Pressure sensors in experiments and CFD simulations can give different results for several reasons, which include model assumption, boundary conditions, mesh resolution (especially in turbulence modeling), flow complexity, and solver convergence. Pressure sensors can also cause different percentage errors at various flow rates in experiments due to several factors, which include sensor calibration, dynamic response, sensor range, fluid properties, installation effects, environmental effects, and instrumentation errors, especially instrumentation drift.

Table 5
Centrifugal pump parameters.

Centrifugal pump parameter	Value
Flow rate	10 m^3/h
Pressure head	632 kPa
Rotational speed	2927 rpm
Liquid to be pumped	Water
Liquid temperature during use	20 °C
Density	998.2 kg/m^3
Pump efficiency	68.6 %
Aggregate efficiency	60 %

5. Conclusion

The integration of CFD simulations and experimental validation in this study underscores its commitment to methodological rigor and practical relevance. By achieving strong agreement between numerical and experimental results, this work validates the reliability of the Realizable k-ε turbulence model for predicting flow dynamics in AJPs. This innovative approach provides a comprehensive framework for optimizing AJP designs, addressing gaps in existing research, and enhancing industrial applications such as slurry pumping and fluid handling. The dual emphasis on theoretical insights and experimental confirmation ensures that the findings are both robust and actionable, demonstrating a significant advancement in the field of jet pump technologies. This paper's CFD simulation scheme represents a carefully crafted and rigorously tested approach. It has been meticulously designed and thoroughly validated by comparing it with experimental data and literature results. This demanding process of verification and calibration instills a high degree of confidence in the accuracy and dependability of the proposed results. The current research paper has developed and validated the CFD scheme using experimental data and literature results, guaranteeing the proposed outcomes' trustworthiness. A parametric study is carried out, which observes variation of suction pressure (P) with fluid flow rate (Q), convergence angle (α), and throat diameter (r_T). Suction pressure shows a direct relationship with fluid flow rate, but this depends on the capacity of the centrifugal pump used. It is observed through the CFD results and experimental work that a reasonable estimate of area ratio and length can be obtained for maximum suction pressure in the venturi pump. Moreover, variation in the throat diameter and length can bring the maximum change in the results. Still, if the secondary fluid changes other than water, this system will fall into the category of slurry. Then, the size of the other fluid particle will also affect the maximum suction capacity.

According to the results above, the following conclusions can be drawn:

1. The maximum fluid flow rate used for this parametric study is 10 m^3/h, which is also quite suitable for the ultimate goal of slurry extraction.

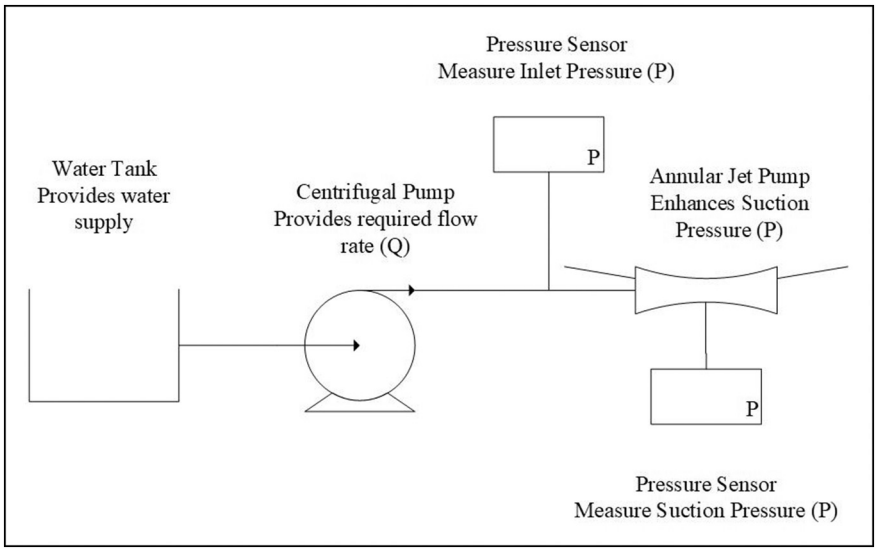

Fig. 9. Schematic of experimental setup.

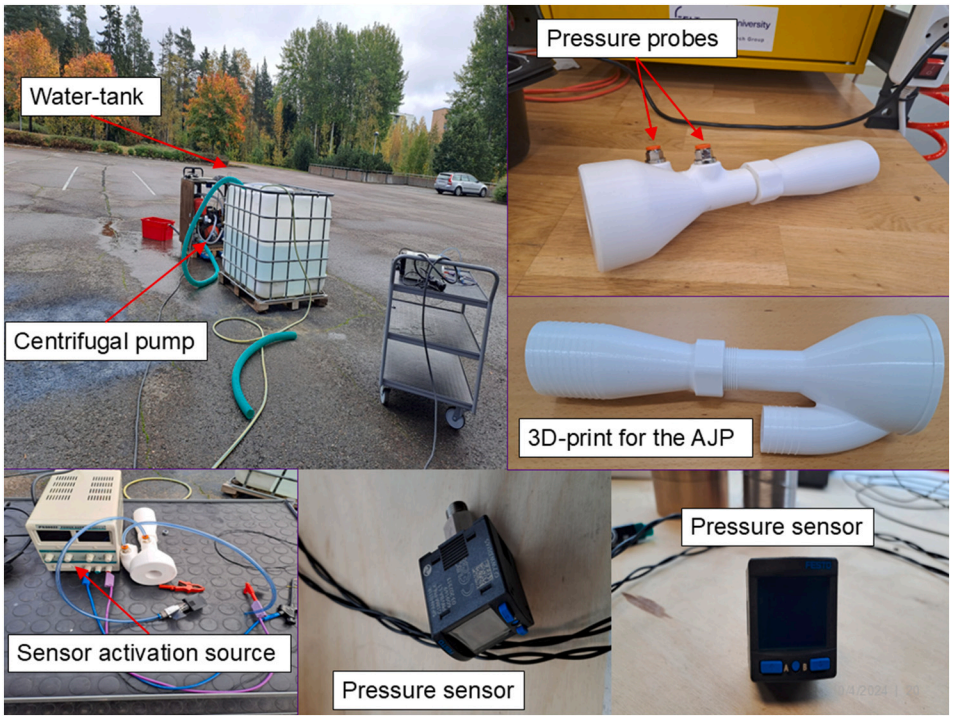

Fig. 10. Real time physical testing visuals.

2. The effects of variation in the converging angle of nozzles are studied for suction pressure, and it is observed that it has a significant impact on the suction pressure and the turbulent kinetic energy, so keeping it in a moderate range will give the optimized flow.
3. Varying the throat diameter (r_T) prominently changes suction pressure; reducing it significantly increases it. However, as this work is intended for slurry modeling, it's essential to consider that slurry particles have different sizes and shapes, so reducing r_T very much is not recommended.

The findings from this study have significant industrial implications. The optimized configuration of throat diameter (10 mm) and convergence angle (27°), resulting in a 34.6 % improvement in suction pressure, is particularly relevant for fluid transport, mining, and dredging applications. These improvements can reduce energy consumption, enhance operational reliability, and increase the efficiency of processes requiring the handling of homogeneous fluids. The robust CFD-experimental framework provides practical guidelines for industrial applications, offering a scalable approach for optimizing AJP designs.

Experimental work validates the parametric study by CFD simulation. Pressure sensors utilized in experimental work possess an accuracy of 1.5 % Full Scale (FS). Although experimental data can vary from simulated values, it lies within the acceptable range. Also, this work is compared with the previous, and no obvious deviation is observed in the results, as discussed in detail in the previous section. Aligning the simulation with real-world experimental data is a critical validation step and ensures that the computational model accurately captures the underlying physical phenomena. This alignment bridges the gap between

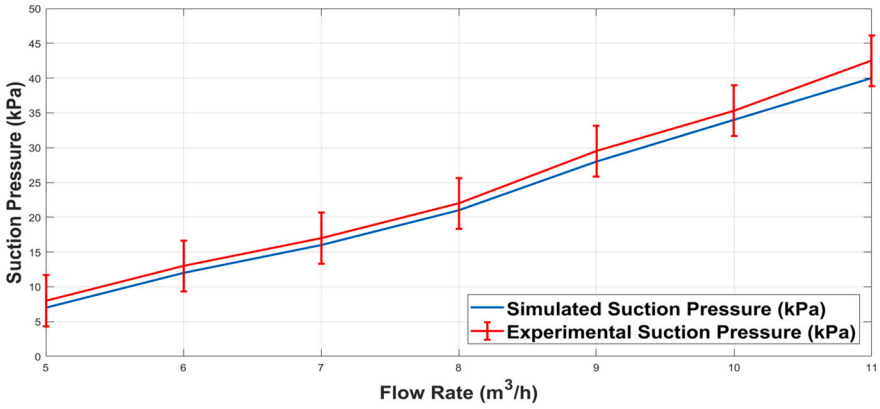

Fig. 11. Comparison of experimental and CFD simulated suction pressure.

theoretical predictions and practical observations, making the CFD simulations a robust tool for various applications, from engineering design to scientific research.

Due to the AJP's high vacuum capability and self-priming performance, it holds significant potential for advancement in practical domains like submarine trenching and dredging. It is especially well-suited for pumping heterogeneous fluids containing substantial quantities of solid particles such as ore, live fish, capsules, industrial waste, and more. While this study provides critical insights, it acknowledges certain limitations. The focus was on single-phase flow, excluding multiphase flow effects commonly encountered in industrial applications like slurry transport. Additionally, the experimental setup used water as both primary and secondary fluids, which limits its direct applicability to more complex fluid systems. In efficient mining, the AJPs play a crucial role, so an optimized geometry can offer great suction capacity, leading to higher efficiency and minimum Specific Energy consumption.

Future research should explore optimizing AJP designs for multiphase flows, accounting for parameters such as particle size, concentration, and their impact on suction performance. Employing advanced turbulence models, such as Large Eddy Simulation (LES) or hybrid approaches, could further refine the accuracy of flow dynamics predictions. For future studies, hybrid models or LES can be employed to further refine the understanding of localized flow phenomena, especially in applications involving more complex multiphase or highly transient flow conditions. Incorporating these advanced modeling techniques can provide deeper insights while complementing the realizable k-ε model's strengths in computational efficiency and broader flow dynamics.

Expanding the experimental setup to include multiphase flow capabilities will bridge the gap between theoretical predictions and practical applications, ensuring the broader industrial relevance of AJPs. In that case, the slurry will be modeled using a multiphase model of COMSOL Multiphysics. The above study can be extended for the multiphase flow, where the secondary fluid can be modeled as slurry. For multiphase flow (slurry extraction in mining), the throat diameter will play a crucial role because it will depend on the size of the secondary fluid particle, which will restrict the size of the throat diameter. Eulerian-Eulerian multiphase model or mixture model can be used to model the multiphase flow, and different turbulence models (Standard k-ε, Realizable k-ε, RNG k-ε, Standard k-ω, and SST k-ω) can be combined to study the flow behavior and turbulence parameters in AJP extensively.

Nomenclature/abbreviations

Symbol	Description	Unit
L_C	length of converging section of the nozzle	mm
L_T	length of the nozzle throat	mm
L_D	length of a diverging section of the nozzle	mm
L	total length of the nozzle	mm
r_T	throat radius of the nozzle	mm
r_i	inlet radius of the nozzle	mm
r_o	outlet radius of the nozzle	mm
α	converging angle of the nozzle	degree
β	diverging angle of the nozzle	degree
u_i	velocity component	m/s
x_i	space coordinate	mm
δ	boundary layer thickness	mm
μ	dynamic viscosity	Pa-s
μ_t	turbulent viscosity	m^2/s
k	turbulence kinetic energy	$m^2 \cdot s^{-2}$
S	strain rate magnitude	s^{-1}
Gk	generation of turbulence kinetic energy due to the mean velocity gradients	$m^2 \cdot s^{-2}$
Gb	generation of turbulence kinetic energy due to buoyancy	$m^2 \cdot s^{-2}$
Ym	contribution of the fluctuating dilatation in compressible turbulence to the overall dissipation rate	mm
σ_k	turbulent Prandtl numbers for k (1.0)	
σ_ε	turbulent Prandtl numbers for ε (1.3)	
S_k, S_ε	user-defined source terms	$m^2 \cdot s^{-3}$
Ωij	mean rate-of-rotation tensor	s^{-1}
A_P	cross sectional area for primary flow	mm^2
A_S	cross sectional area for secondary flow	mm^2

CRediT authorship contribution statement

Sadia Riaz: Writing – original draft, Validation, Software, Methodology, Investigation, Formal analysis, Conceptualization. **Jussi Aaltonen:** Writing – review & editing, Visualization, Project administration, Funding acquisition. **Tobias Pinkse:** Visualization, Resources, Conceptualization. **Kari Koskinen:** Writing – review & editing, Supervision, Resources, Project administration, Investigation, Funding acquisition, Data curation, Conceptualization.

Declaration of competing interest

The authors declare that they have no known competing financial interests or personal relationships that could have appeared to influence the work reported in this paper.

Acknowledgments

This project has received funding from the European Union's Horizon 2020 research and innovation program under grant agreement 820971.

Data availability

Data will be made available on request.

References

[1] J. Singh, S. Catsoulis, D. Lakehal, C. Narayanan, Predicting pressure-drop for pseudo-homogeneous slurry flows using the mixture model at high solids concentrations, Int. J. Multiphase Flow 159 (Feb. 2023), https://doi.org/10.1016/j.ijmultiphaseflow.2022.104339.

[2] J. Fan, et al., Computational fluid dynamic analysis and design optimization of jet pumps, Comput. Fluids 46 (1) (Jul. 2011) 212–217, https://doi.org/10.1016/j.compfluid.2010.10.024.

[3] M.A. Kökpinar, M. Göğüş, The performance of water jet pumps and their application in slurry transportation, Isi Bilimi Ve Tek. Derg./J. Ther. Sci. Technol. 43 (1) (2023) 119–134, https://doi.org/10.47480/isibted.1290753.

[4] K. Xu, et al., Parameter analysis and optimization of annular jet pump based on kriging model, Appl. Sci. (Switzerland) 10 (21) (Nov. 2020) 1–16, https://doi.org/10.3390/app10217860.

[5] R. Yapici, K. Aldaş, Optimization of water jet pumps using numerical simulation, Proc. Inst. Mech. Eng. Pt. A J. Power Energy 227 (4) (Jun. 2013) 438–449, https://doi.org/10.1177/0957650913487529.

[6] T. Meakhail, I. Teaima, Experimental and numerical studies of the effect of area ratio and driving pressure on the performance of water and slurry jet pumps, Proc. Inst. Mech. Eng. C J. Mech. Eng. Sci. 226 (9) (Sep. 2012) 2250–2266, https://doi.org/10.1177/0954406211430458.

[7] S. Nakamura, S. Kuzuhara, S.K. Teacher, Yukimaru Shimizu studies of the configuration and performance of annular type jet pumps [Online]. Available: http://asmedigitalcollection.asme.org/fluidsengineering/article-pdf/109/3/205/5751567/205_1.pdf, 1987.

[8] O.B. Kwon, M.K. Kim, H.C. Kwon, D.S. Bae, Two-dimensional Numerical Simulations on the Performance of an Annular Jet Pump, 2002.

[9] Z. Wang, Y. Lei, Z. Wu, J. Wu, M. Zhang, R. Liao, Structure size optimization and internal flow field analysis of a new jet pump based on the Taguchi method and numerical simulation, Processes 11 (2) (Feb. 2023), https://doi.org/10.3390/pr11020341.

[10] M. Sen Xu, X.L. Yang, X.P. Long, Q. Lyu, B. Ji, Numerical investigation of turbulent flow coherent structures in annular jet pumps using the LES method, Sci. China Technol. Sci. 61 (1) (Jan. 2018) 86–97, https://doi.org/10.1007/s11431-017-9047-8.

[11] Q. Lyu, Z. Xiao, Q. Zeng, L. Xiao, X. Long, Implementation of design of experiment for structural optimization of annular jet pumps, J. Mech. Sci. Technol. 30 (2) (Feb. 2016) 585–592, https://doi.org/10.1007/s12206-016-0112-y.

[12] X. Deng, J. Dong, Z. Wang, J. Tu, Numerical analysis of an annular water-air jet pump with self-induced oscillation mixing chamber, J. Comput. Multiphase Flows 9 (1) (Mar. 2017) 47–53, https://doi.org/10.1177/1757482X16688476.

[13] L.Z. Xiao, X.P. Long, Q. Lyu, Y. Hu, Q.Q. Wang, Numerical investigation on the cavitating flow in annular jet pump under different flow rate ratio, in: IOP Conference Series: Earth and Environmental Science, Institute of Physics Publishing, 2014, https://doi.org/10.1088/1755-1315/22/5/052001.

[14] M. Sen Xu, X. Long Yang, X. Ping Long, Q. Lü, Large eddy simulation of turbulent flow structure and characteristics in an annular jet pump, J. Hydrodyn. 29 (4) (Aug. 2017) 702–715, https://doi.org/10.1016/S1001-6058(16)60782-5.

[15] C.H. Zou, Effect of structural forms on the performance of a jet pump for a deep well jet pump, in: Computational Methods and Experimental Measurements XVII, WIT Press, May 2015, pp. 257–266, https://doi.org/10.2495/cmem150231.

[16] H. Safikhani, A. Khalkhali, M. Farajpoor, Pareto based multi-objective optimization of centrifugal pumps using CFD, neural networks and genetic algorithms, Eng. Appl. Comput. Fluid Mech. 5 (1) (2011) 37–48, https://doi.org/10.1080/19942060.2011.11015351.

[17] Z. An, L. Zhounian, W. Peng, C. Linlin, W. Dazhuan, Multi-objective optimization of a low specific speed centrifugal pump using an evolutionary algorithm, Eng. Optim. 48 (7) (Jul. 2016) 1251–1274, https://doi.org/10.1080/0305215X.2015.1104987.

[18] M. Nasr, M.A. Hosien, E.M. Wahba, A.A.A. Sheha, Computational and Experimental Study on the Water-jet Pump Performance Under Different Geometrical and Operational Parameters, 2017.

[19] Z. Xu-He, Y. Ting-Jun, W. Xiao-He, Influence of Different Turbulence Models on Flow Field Simulation of Nozzle Adjustable Jet Pump, 2017.

[20] A. Morrall, S. Quayle, M.S. Campobasso, Turbulence modelling for RANS CFD analyses of multi-nozzle annular jet pump swirling flows, Int. J. Heat Fluid Flow 85 (Oct. 2020), https://doi.org/10.1016/j.ijheatfluidflow.2020.108652.

[21] K. Xu, et al., CFD-based study of nozzle section geometry effects on the performance of an annular multi-nozzle jet pump, Processes 8 (2) (Feb. 2020), https://doi.org/10.3390/pr8020133.

[22] K. Xu, et al., Parameter analysis and optimization of annular jet pump based on kriging model, Appl. Sci. (Switzerland) 10 (21) (Nov. 2020) 1–16, https://doi.org/10.3390/app10217860.

[23] Z. Wang, Y. Lei, Z. Wu, J. Wu, M. Zhang, R. Liao, Structure size optimization and internal flow field analysis of a new jet pump based on the Taguchi method and numerical simulation, Processes 11 (2) (Feb. 2023), https://doi.org/10.3390/pr11020341.

[24] A. Morrall, S. Quayle, M.S. Campobasso, Turbulence modelling for RANS CFD analyses of multi-nozzle annular jet pump swirling flows, Int. J. Heat Fluid Flow 85 (Oct. 2020), https://doi.org/10.1016/j.ijheatfluidflow.2020.108652.

[25] R. Shaheed, A. Mohammadian, H. Kheirkhah Gildeh, A comparison of standard k–ε and realizable k–ε turbulence models in curved and confluent channels, Environ. Fluid Mech. 19 (2) (Apr. 2019) 543–568, https://doi.org/10.1007/s10652-018-9637-1.

[26] X. Wang, Y. Chen, M. Li, Y. Xu, B. Wang, X. Dang, Numerical study on the working performance of a streamlined annular jet pump, Energies (Basel) 13 (17) (Sep. 2020), https://doi.org/10.3390/en13174411.

[27] I.A. Idowu, M.O. Olayiwola, A.W. Gbolagade, Relationship between continuity and momentum equation in two dimensional flow [Online]. Available: http://www.sciencepub.net, 2009.

[28] A. Sana, A.R. Ghumman, H. Tanaka, Modification of the damping function in the k-ε model to analyse oscillatory boundary layers, Ocean Eng. 34 (2) (Feb. 2007) 320–326, https://doi.org/10.1016/j.oceaneng.2005.11.018.